Modeling of Wave Propagation in Layered Piezoelectric Media by a Recursive Asymptotic Method

Lugen Wang, *Member, IEEE*, and Stanislav I. Rokhlin

***Abstract*—In this paper, a simple asymptotic method to compute wave propagation in a multilayered general anisotropic piezoelectric medium is discussed. The method is based on explicit second and higher order asymptotic representations of the transfer and stiffness matrices for a thin piezoelectric layer. Different orders of the asymptotic expansion are obtained using Padé approximation of the transfer matrix exponent. The total transfer and stiffness matrices for thick layers or multilayers are calculated with high precision by subdividing them into thin sublayers and combining recursively the thin layer transfer and stiffness matrices. The rate of convergence to the exact solution is the same for both transfer and stiffness matrices; however, it is shown that the growth rate of the round-off error with the number of recursive operations for the stiffness matrix is twice that for the transfer matrix; and the stiffness matrix method has better performance for a thick layer. To combine the advantages of both methods, a hybrid method which uses the transfer matrix for the thin layer and the stiffness matrix for the thick layer is proposed. It is shown that the hybrid method has the same stability as the stiffness matrix method and the same round-off error as the transfer matrix method. The method converges to the exact transfer/stiffness matrices essentially with the precision of the computer round-off error. To apply the method to a semispace substrate, the substrate was replaced by an artificial perfect matching layer. The computational results for such an equivalent system are identical with those for the actual system. In our computational experiments, we have found that the advantage of the asymptotic method is its simplicity and efficiency.**

I. Introduction

Recently [1] we proposed a simple asymptotic method to compute wave propagation in layered piezoelectric media. The method uses an explicit second order asymptotic representation [2] for the transfer matrix of a thin anisotropic layer and uses it recursively to obtain general Green's functions in a layered piezoelectric system. The advantage of the method is that one does not need to compute the exact wave propagation solution for each anisotropic layer of the system, and only the elastic, piezoelectric, and dielectric constants of the layers are required. Compared to the exact [3]–[6] and approximate finite-element methods [7]–[9], this method is much simpler and computationally efficient.

Manuscript received May 23, 2003; accepted May 26, 2004.

The authors are with The Ohio State University, Nondestructive Evaluation Program, Edison Joining Technology Center, Columbus, OH 43221 (e-mail: rokhlin.2@osu.edu).

This paper further extends the foundations and application of the method. In Section II, the second and higher order solutions based on the Padé approximation will be introduced. The computational error due to the layer subdivision into $N = 2^n$ thin layers and computer rounding error will be analyzed, and a simple equation for the optimal number of subdivisions N will be derived. A hybrid method that combines the low-rounding-error transfer matrix and the unconditionally stable stiffness matrix methods will be developed; as a result it has low rounding error and no computational instabilities at high frequency. In Section III, the perfect match layer (PML) method will be developed to compute the surface stiffness matrix for a semispace. It will be shown that this method is inapplicable in the angle domain in which the phase and group velocities of the quasitransverse partial wave in the semispace have opposite directions. How to overcome these difficulties and a simple criterion to identify those domains will be shown. In Section IV the application of this method to compute the surface Green's function and surface acoustic wave velocities will be given.

II. Asymptotic Computation Method for a Thin Layer

A. Exact Transfer Matrix and Second Order Asymptotic Transfer Matrix

Let us consider generally anisotropic piezoelectric media as shown in Fig. 1. We define the general displacement $\mathbf{U}(=[\mathbf{u},\phi]^{\mathrm{T}})$ and general stress $\mathbf{T}=[\boldsymbol{\sigma},D_3]^{\mathrm{T}}$ vectors and the state vector $\xi=\begin{bmatrix}\mathbf{U}\\ \mathbf{T}\end{bmatrix}$, where $\mathbf{u}$ and $\boldsymbol{\sigma}$ are the particle displacement and normal stress vectors, respectively, and ϕ and D_3 are the electric potential and normal electric displacement, respectively. The general solution for the state vector can be represented in the form $\xi(z)e^{i(\omega t-k_x x)}$, where ω is angular frequency, k_x is wave number along the x axis. The governing equation for the state vector is [3], [4], [6]:

$$\frac{d\xi}{dz}=i\mathbf{A}\xi, \tag{1}$$

where $\mathbf{A}$ is the fundamental acoustic tensor given by Fahmy and Adler [3] (see also Appendix A). For a single homogeneous layer, the differential (1) has the well-known exponential transfer matrix solution $\mathbf{B}$, which relates the

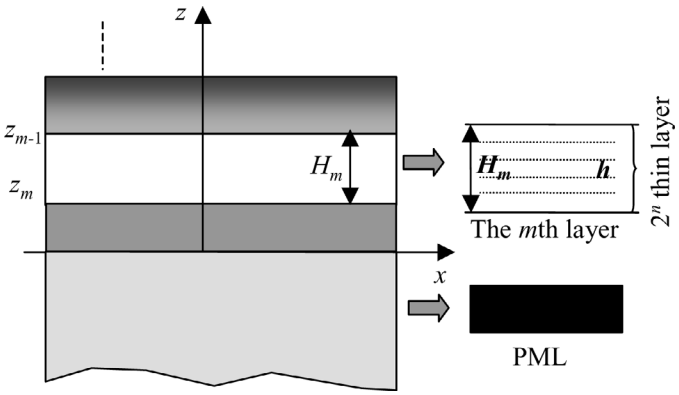

Fig. 1. Schematic of a layered structure and coordinate system. Each layer is subdivided into 2^n thin layers with the same thickness h. The semispace substrate is replaced by the PML. The layered system also may include functionally graded layers.

state vector at the layer top $(z+h)$ to that at the layer bottom (z) surface:

$$\xi(z+h) = \mathbf{B}\xi(z), \quad \mathbf{B} = e^{i\mathbf{A}h}, \tag{2}$$

where h is the layer thickness. To compute $\mathbf{B}$ requires finding the eigenvalues and eigenvectors of the fundamental matrix $\mathbf{A}$ [3], [4].

For a thin layer $h/\lambda \ll 1$, a second-order asymptotic approximation for the transfer matrix (2) has been proposed by Rokhlin and Huang [2], which can be written as:

$$\mathbf{B}_{\mathrm{II}} = \left(\mathbf{I} - i\frac{h}{2}\mathbf{A}\right)^{-1}\left(\mathbf{I} + i\frac{h}{2}\mathbf{A}\right). \tag{3}$$

Comparing the series expansion for the transfer matrix $\mathbf{B}$ from (2) and (3), one concludes that they differ in the third order term, thus the absolute error is of order $(h\mathbf{A})^3$. The advantage of the asymptotic transfer matrix representation (3) is that it has the same symmetry properties as the exact transfer matrix, and the wave solution obtained with the transfer matrix (3) satisfies energy balance for wave interaction with a thin layer [2]. As was shown in [2], this is due inherently to the representation of the transfer matrix $\mathbf{B}_{\mathrm{II}}$ in the form (3). The series representation of matrix $\mathbf{B}$ (2) to any order will not satisfy energy balance exactly. Note 1. It is very important to note that an artificially selected layer in the homogeneous solid described by the asymptotic transfer matrix (3) does not introduce any scattering in the structure independently of the layer thickness [2].

B. Convergence of the Asymptotic Matrix $\mathbf{B}_{\mathrm{II}}$ to the Exact Transfer Matrix

The asymptotic solutions derived above are valid only for a thin layer. For a thick layer with thickness H, one can subdivide it into N thin layers, and the total asymptotic transfer matrix $\mathbf{B}_a(H)$ for a thick layer is obtained as the product of all thin layer transfer matrices

$$\mathbf{B}_a(H) = [\mathbf{B}_{\mathrm{II}}(h)]^N. \tag{4}$$

To show the convergence of the asymptotic transfer matrix $\mathbf{B}_a(H)$ to the exact one, we substitute the asymptotic transfer matrix (3) into (4):

$$\mathbf{B}_a(H) = \left[\left(\mathbf{I} - \frac{iH\mathbf{A}}{2N}\right)^{-1}\left(\mathbf{I} + \frac{iH\mathbf{A}}{2N}\right)\right]^N. \tag{5}$$

Because $\left(\mathbf{I} - \frac{iH\mathbf{A}}{2N}\right)^{-1}$ and $\left(\mathbf{I} + \frac{iH\mathbf{A}}{2N}\right)$ commute [2], (5) can be written as $\mathbf{B}_a(H) = \left[\left(\mathbf{I} - \frac{iH\mathbf{A}}{2N}\right)^{-1}\right]^N \left[\left(\mathbf{I} + \frac{iH\mathbf{A}}{2N}\right)\right]^N$. Because $\left(e^{-iH\mathbf{A}/2}\right)^{-1} = e^{iH\mathbf{A}/2}$, and $e^{iH\mathbf{A}/2}e^{iH\mathbf{A}/2} = e^{iH\mathbf{A}}$, the approximate transfer matrix $\mathbf{B}_a(H)$ converges to the exact transfer matrix $\mathbf{B}(H) = e^{i\mathbf{A}H}$ as the number of subdivisions N approaches infinity.

For computational efficiency, one should select N as a power of 2 $(N = 2^n)$, then for a homogeneous layer H the number of matrix multiplications is n if $\mathbf{B}_a$ is calculated recursively as:

$$\mathbf{B}_a^{(J)} = \mathbf{B}_a^{(J-1)}\mathbf{B}_a^{(J-1)}, \tag{6}$$

where $(J) = (1), \ldots (n)$ is a running index; $\mathbf{B}_a^{(0)} = \mathbf{B}_{\mathrm{II}}(h)$; $\mathbf{B}_a^{(J)} = \mathbf{B}_a(2^j h)$ is the total asymptotic transfer matrix at step J; $\mathbf{B}_a^{(J-1)} = \mathbf{B}_a(2^{j-1}h)$ and $H = 2^n h$. Note 2. As a consequence of zero scattering of the asymptotic layer representation in a homogeneous solid (Note 1) the discretization (4) maintains the homogeneity of the layer H. This homogeneity is independent of the number of subdivisions N, i.e., the subdivision does not introduce discretization-type artifacts into the solution. Of course, the precision of the approximation of the total matrix $\mathbf{B}_a$ elements will depend on N.

To assess the precision of the method, we define the relative error $E(\mathbf{B})$ as the average relative error between the asymptotic and exact transfer matrix elements $\mathbf{B}[i, j]$:

$$E(\mathbf{B}) = \frac{1}{64}\sum_{i=1}^{8}\sum_{j=1}^{8}\left|\left(\mathbf{B}_a[i, j] - \mathbf{B}[i, j]\right)/\mathbf{B}[i, j]\right|. \tag{7}$$

To investigate the convergence rate and the accumulation of round-off error with the increase of a number of subdivisions $N = 2^n$, we plot in Fig. 2 (open triangles) the average relative error versus number of recursive operations n at 1 GHz for a ZnO layer with thickness $H = 1$ μm. $E(\mathbf{B})$ is averaged for a phase velocity (ω/k_x) in the range between 1.0 and 20.0 mm/μs. The calculation is performed with double precision. One can see that initially the relative error decreases exponentially as $(H/2^n)^2$ with an increase of number of recursive operations n. This is because, with an increase of n, the thickness of the subdivision layers $h = H/2^n$ exponentially decreases for a given H, which leads to an exponential decrease of the truncation error. As the number of recursive operations reaches a critical point, the error starts to increase due to the accumulation of round-off error [10], resulting from multiplication of a large number of asymptotic transfer matrices. The growth rate of the round-off error is proportional to 2^n.

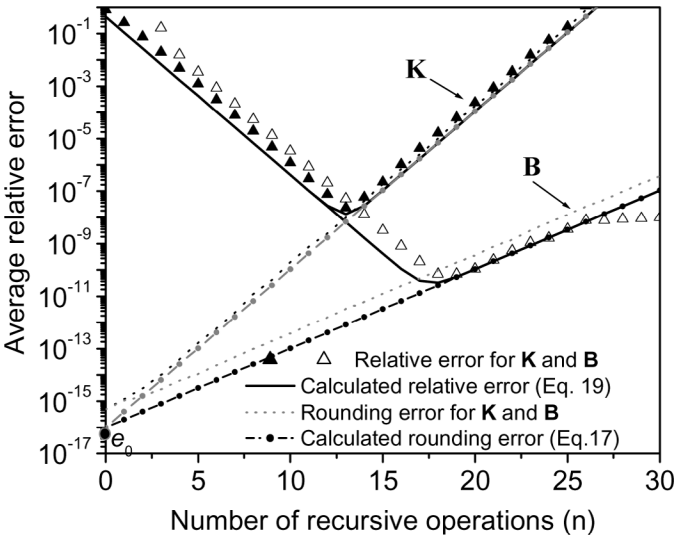

Fig. 2. Comparison of simulated (19) and actual relative error for stiffness (**K**) and transfer (**B**) matrices calculated by the asymptotic method for a ZnO layer at $fH = 1$ GHz$^*\mu$m. The number of layer subdivisions N is 2^n. The relative error averaged in the phase-velocity (ω/k_x) range between 1.0 and 20.0 mm/μs. Dotted lines are for the rounding error for **K** and **B** calculated using the exact method, and dashed lines with dots are rounding errors estimated using (17).

The growth and decay rates are independent of the layer thickness H and its material and in this sense are universal. For each layer thickness, there is an optimal number N of subdivisions for which the average relative error is minimal.

C. Higher Order Asymptotic Transfer Matrix

In the previous sections, we describe an asymptotic solution based on the second order approximation of the transfer matrix. Higher order solutions can be obtained using the Cayley transform or the Padé approximation [11]. Detailed discussion of the higher order Padé approximation together with Magnus expansion for wave propagation in a functionally graded multilayered medium is given in [11].

The 2m-th order diagonal Padé approximation for the transfer matrix (2) is

$$\mathbf{B}_{2m} = \left(\Xi_m(-ih\mathbf{A})\right)^{-1}\left(\Xi_m(ih\mathbf{A})\right), \tag{8}$$

the matrix polynomials $\Xi_m(ih\mathbf{A})$ are generated according to the recurrence:

$$\Xi_0(ih\mathbf{A}) = 1, \;\; \Xi_1(ih\mathbf{A}) = 2 + ih\mathbf{A}, \tag{9}$$
$$\Xi_m(ih\mathbf{A}) = 2(2m-1)\Xi_{m-1}(ih\mathbf{A}) - (h\mathbf{A})^2\Xi_{m-2}(ih\mathbf{A}).$$

The second order approximation ($m = 2$) is identical with (3). The fourth, sixth, and eighth order solutions are given by (10) (see next page).

As does the second order solution, the higher order approximation preserves the symmetry properties of the exact transfer and stiffness matrices, and the wave solution obtained with these asymptotic matrices satisfies energy balance for wave interaction with a thin layer [11].

Higher order solutions also may be obtained using convergence-accelerating techniques such as Richardson extrapolation or epsilon extrapolation algorithms [12]. The solution obtained using epsilon extrapolation is identical to the Padé approximation described above. The fourth order Richardson extrapolation for the transfer matrix is:

$$\mathbf{B}^R_{\mathrm{IV}}(h) = \frac{4}{3}\mathbf{B}_{\mathrm{II}}(h/2)\mathbf{B}_{\mathrm{II}}(h/2) - \frac{1}{3}\mathbf{B}_{\mathrm{II}}(h), \tag{11}$$

where $\mathbf{B}_{\mathrm{II}}$ is given by (3). The accuracy and computational complexity of the fourth order Richardson approximation (11) is similar to the fourth order Padé approximation (10a). However, solutions based on (11) do not satisfy energy balance exactly.

D. Asymptotic Stiffness Matrix Method

For high fH the precision of the transfer matrix computation decreases, and it is advantageous to use the stiffness matrix method [5], [6]. To obtain the asymptotic stiffness matrix from the general asymptotic transfer matrix, we use the relation between the transfer matrix **B** and the stiffness matrix **K** [5], [6]:

$$\mathbf{K} = \begin{bmatrix} \mathbf{B}_{22}\left(\mathbf{B}_{12}\right)^{-1} & \mathbf{B}_{21} - \mathbf{B}_{22}\left(\mathbf{B}_{12}\right)^{-1}\mathbf{B}_{11} \\ \left(\mathbf{B}_{12}\right)^{-1} & -\left(\mathbf{B}_{12}\right)^{-1}\mathbf{B}_{11} \end{bmatrix}. \tag{12}$$

Substituting the second order transfer matrix $\mathbf{B}_{\mathrm{II}}$ (3) into (12) and using the submatrices $\mathbf{\Gamma}_{ik}$ in the acoustic tensor **A** (Appendix A), the second-order stiffness matrix $\mathbf{K}_{\mathrm{II}}$ is obtained explicitly as (13) (see next page).

The expanded form of the second-order stiffness matrix (13) for conductive isotropic layers is given in Appendix B. The asymptotic stiffness matrix elements are simple, explicit functions of the elastic, piezoelectric and dielectric properties.

The 2m-th order approximation to the stiffness matrix $\mathbf{K}_{2\mathrm{m}}$ is obtained in terms of the submatrices $\mathbf{\Xi}^{ij}_m$ of $\mathbf{\Xi}_m$ from the high order asymptotic transfer matrix (8) using (12):

$$\mathbf{K}_{2\mathrm{m}} = \begin{bmatrix} -\mathbf{\Xi}^{12}_m(ih\mathbf{A}) & \mathbf{\Xi}^{12}_m(ih\mathbf{A}) \\ -\mathbf{\Xi}^{22}_m(ih\mathbf{A}) & \mathbf{\Xi}^{22}_m(ih\mathbf{A}) \end{bmatrix}^{-1} \begin{bmatrix} \mathbf{\Xi}^{11}_m(ih\mathbf{A}) & -\mathbf{\Xi}^{11}_m(ih\mathbf{A}) \\ \mathbf{\Xi}^{21}_m(ih\mathbf{A}) & -\mathbf{\Xi}^{21}_m(ih\mathbf{A}) \end{bmatrix}. \tag{14}$$

To find the stiffness matrix of a thick layer as discussed above, the thick layer H is subdivided into $N = 2^n$ thin layers $h = H/N$, and the total stiffness matrix of the thick layer is obtained from the thin layer stiffness matrix using a recursive algorithm (see (15), next page) [5], [6], where $J = 1, \ldots n$; $\mathbf{K}^J_a$ is the total asymptotic stiffness matrix after J recursive operations, and $\mathbf{K}^0_{ij}$ are the submatrices of the thin layer asymptotic stiffness matrix $\mathbf{K}_{\mathrm{II}}$ (13) or $\mathbf{K}_{2\mathrm{m}}$ (14). As in the case of the asymptotic transfer matrix, to obtain the total stiffness matrix for $N = 2^n$ subdivisions,

$$\mathbf{B}_{\mathrm{IV}} = \left(\mathbf{I} - \frac{1}{2}ih\mathbf{A} + \frac{1}{12}(ih\mathbf{A})^2\right)^{-1}\left(\mathbf{I} + \frac{1}{2}ih\mathbf{A} + \frac{1}{12}(ih\mathbf{A})^2\right), \tag{10a}$$

$$\mathbf{B}_{\mathrm{VI}} = \left(\mathbf{I} - \frac{1}{2}ih\mathbf{A} + \frac{1}{10}(ih\mathbf{A})^2 - \frac{1}{120}(ih\mathbf{A})^3\right)^{-1}\left(\mathbf{I} + \frac{1}{2}ih\mathbf{A} + \frac{1}{10}(ih\mathbf{A})^2 + \frac{1}{120}(ih\mathbf{A})^3\right), \tag{10b}$$

$$\mathbf{B}_{\mathrm{VIII}} = \left(\mathbf{I} - \frac{1}{2}ih\mathbf{A} + \frac{3}{28}(ih\mathbf{A})^2 - \frac{1}{84}(ih\mathbf{A})^3 + \frac{1}{1680}(ih\mathbf{A})^4\right)^{-1}\left(\mathbf{I} + \frac{1}{2}ih\mathbf{A} + \frac{3}{28}(ih\mathbf{A})^2 + \frac{1}{84}(ih\mathbf{A})^3 + \frac{1}{1680}(ih\mathbf{A})^4\right). \tag{10c}$$

$$\mathbf{K}_{\mathrm{II}} = \begin{bmatrix} \frac{\mathbf{\Gamma}_{33}}{h} - (\mathbf{\Gamma}_{31} - \mathbf{\Gamma}_{13})\frac{ik_x}{2} + \frac{\mathbf{\Gamma}_{11}hk_x^2}{4} - \frac{\rho h\omega^2}{4}\mathbf{I}' & -\frac{\mathbf{\Gamma}_{33}}{h} - (\mathbf{\Gamma}_{31} + \mathbf{\Gamma}_{13})\frac{ik_x}{2} + \frac{\mathbf{\Gamma}_{11}hk_x^2}{4} - \frac{\rho h\omega^2}{4}\mathbf{I}' \\ \frac{\mathbf{\Gamma}_{33}}{h} - (\mathbf{\Gamma}_{31} + \mathbf{\Gamma}_{13})\frac{ik_x}{2} - \frac{\mathbf{\Gamma}_{11}hk_x^2}{4} + \frac{\rho h\omega^2}{4}\mathbf{I}' & -\frac{\mathbf{\Gamma}_{33}}{h} - (\mathbf{\Gamma}_{31} - \mathbf{\Gamma}_{13})\frac{ik_x}{2} - \frac{\mathbf{\Gamma}_{11}hk_x^2}{4} + \frac{\rho h\omega^2}{4}\mathbf{I}' \end{bmatrix}. \tag{13}$$

$$\mathbf{K}_a^J = \begin{bmatrix} \mathbf{K}_{11}^{J-1} + \mathbf{K}_{12}^{J-1}\left(\mathbf{K}_{11}^{J-1} - \mathbf{K}_{22}^{J-1}\right)^{-1}\mathbf{K}_{21}^{J-1} & -\mathbf{K}_{12}^{J-1}\left(\mathbf{K}_{11}^{J-1} - \mathbf{K}_{22}^{J-1}\right)^{-1}\mathbf{K}_{12}^{J-1} \\ \mathbf{K}_{21}^{J-1}\left(\mathbf{K}_{11}^{J-1} - \mathbf{K}_{22}^{J-1}\right)^{-1}\mathbf{K}_{21}^{J-1} & \mathbf{K}_{22}^{J-1} - \mathbf{K}_{21}^{J-1}\left(\mathbf{K}_{11}^{J-1} - \mathbf{K}_{22}^{J-1}\right)^{-1}\mathbf{K}_{12}^{J-1} \end{bmatrix}, \tag{15}$$

only n recursive operations are required. Because (13) is uniquely related to (3), the convergence of the recursive algorithm (15) to the exact stiffness matrix follows from the convergence of the operation (4) to the exact transfer matrix solution. However, in contrast to (4), the algorithm of (15) is computationally stable for an arbitrary fH product [6].

To illustrate the convergence rate and the effect of round-off error, as we did for the transfer matrix (7) we calculated the average relative error $E(\mathbf{K})$ as:

$$E(\mathbf{K}) = \frac{1}{64}\sum_{i=1}^{8}\sum_{j=1}^{8}\left|\left(\mathbf{K}_a[i,\,j] - \mathbf{K}[i,\,j]\right)/\mathbf{K}[i,\,j]\right|. \tag{16}$$

The computed $E(\mathbf{K})$ for the second order approximation is shown in Fig. 2 by the solid triangles using the same parameters as those for the $E(\mathbf{B})$ computation. The relative errors for both the second order stiffness and transfer matrices have the same decay rate proportional to $(H/2^n)^2$. The growth rate of the stiffness matrix round-off error is proportional to $(2^n)^2$. Therefore, the minimum error $E(\mathbf{K})_{\min}$ of the stiffness matrix approximation is higher than that of the transfer matrix. This minimum error increases with total thickness increase.

Using the same parameters as for the second order computation shown in Fig. 2, in Fig. 3(a) we have compared the relative error $E(\mathbf{K})$ for the fourth, sixth, and eighth order approximation for the recursive stiffness matrix method (15). As in Fig. 2, after the number of recursive operations reaches a critical point, due to accumulation of the round-off error, the total relative error starts to increase with the number of recursive operations. This increase is independent of approximation order. Due to the existence of two competing effects (the truncation and round-off errors), optimizing the number of recursive operations is important in obtaining a good approximation.

To illustrate the efficiency of the different order approximations, using the same parameters as those for Fig. 3(a), we have recorded the relative error for different order approximations at given computation (CPU) time, then plotted in Fig. 3(b) the average relative error $E(\mathbf{K})$ as function of CPU time. The CPU time is normalized by the CPU time for the eigenvalue-based method. In this calculation, the second order solution is obtained using the explicit form (13). As one can see, the second order approximation is more computationally efficient when medium accuracy is required ($E > 10^{-8}$). When higher accuracy is required, higher order approximations are advantageous.

The exact solution requires finding the eigenvalues and eigenvectors of the fundamental acoustic matrix $\mathbf{A}$. In general, the asymptotic method is more computationally efficient than the exact method as shown in Fig. 3(b). However, for a given relative error, the CPU time for the recursive asymptotic method increases with fH, and that for the eigenvalue- and eigenvector-based method is independent of fH. Because the number of recursive operations n is a logarithmic function of the number of subdivisions N ($n = \log_2 N$), the layer thickness and frequency do not significantly affect the efficiency of the recursive asymptotic method. In the case of absence of acoustic losses using the special form of matrix $\mathbf{A}$, one may replace the complex eigenvalue problem computation by a real eigenvalue problem. In this case the computational efficiency for both methods is similar.

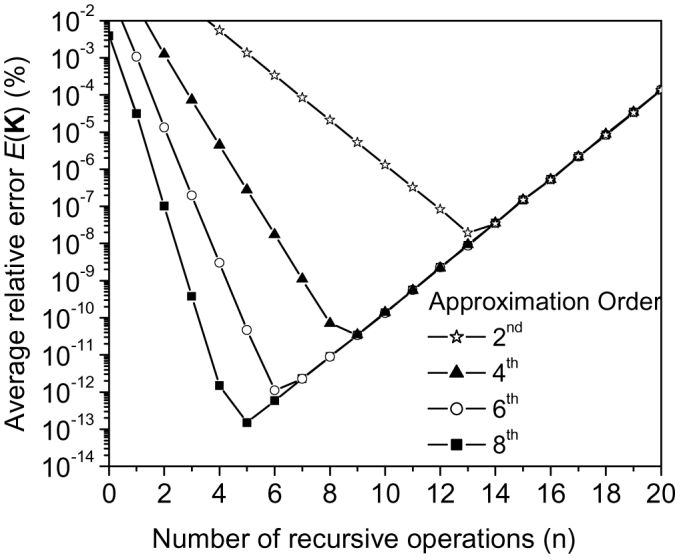

(a)

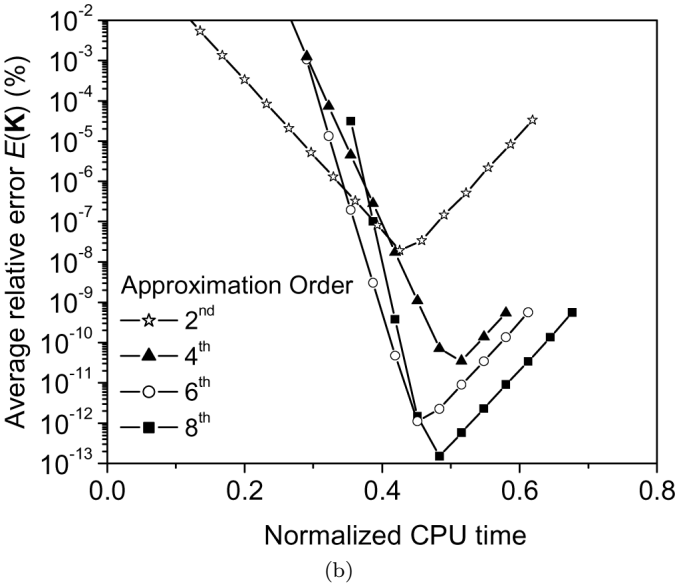

(b)

Fig. 3. (a) Average relative error $E(\mathbf{K})$ versus recursive operation number for different approximation orders. (b) Average relative error $E(\mathbf{K})$ versus normalized CPU time for different approximation order. The CPU time is normalized by the CPU time for the eigenvalue-based method. Computational parameters are the same as in Fig. 2.

E. Error Analysis

As shown in the previous sections, the total relative error is composed from the truncation error that decreases with the number of subdivisions and the round-off error which is dependent on the number of recursive operations; and it increases with this number. Therefore, the relative error has an optimum number of subdivisions that we will estimate analytically.

Let us first perform error analysis for the second order approximation. To investigate the round-off error introduced by the recursive algorithm, we calculated the average relative difference (error) between the exact transfer and stiffness matrices ($\mathbf{B}(H)$, $\mathbf{K}(H)$) for a layer of thickness H and those calculated recursively using the exact (2) thin layer matrices ($\mathbf{B}(h)$, $\mathbf{K}(h)$) instead of the asymptotic thin layer matrices $\mathbf{B}_{\mathrm{II}}(h)$, $\mathbf{K}_{\mathrm{II}}(h)$. Therefore, the difference indicates only the round-off error (the rounding error introduced by the recursive repetition of the exact thin layer matrices). The result is shown by the dotted lines in Fig. 2. By fitting the dotted lines in Fig. 2 with an exponential function, we empirically determine the average relative round-off error for the transfer $E_R(\mathbf{B})$ and stiffness matrices $E_R(\mathbf{K})$ as:

$$E_R(\mathbf{B}) = 2^n e_0,\ E_R(\mathbf{K}) = 4^n e_0, \tag{17}$$

where e_0 is the minimum round-off error of the computer; it is estimated from Fig. 2 to be 10^{-16} for double precision computations. The round-off error estimated using (17) is shown in Fig. 2 by dashed lines with solid dots. As follows from (17), with an increase of the number n of recursive operations, the round-off error of the stiffness matrix has 4^n dependence comparing to 2^n for the transfer matrix. The higher round-off error for the stiffness matrix results from its more complicated recursive operation (15) and need for matrix inversion $(\mathbf{K}_{11} - \mathbf{K}_{22})^{-1}$.

The truncation error (the difference between the exact and the asymptotic solutions) decreases with the number of layer subdivisions. The truncation error is obtained by expanding the elements of both the exact and asymptotic transfer and stiffness matrices in a Taylor series in terms of thin layer thickness [13]. For example, considering wave propagation along the z direction in an orthotropic layer, the exact transfer matrix element $\mathbf{B}[3,7]$ and the asymptotic transfer matrix element $\mathbf{B}_{\mathrm{II}}[3,7]$ are given by:

$$\begin{aligned}\mathbf{B}[3,7] &= \frac{h\sin(\alpha)}{\alpha C_{33}} = \frac{h}{C_{33}}\left(1 - \frac{1}{6}\alpha^2 + O(\alpha^4)\right)\\ \mathbf{B}_{\mathrm{II}}[3,7] &= \frac{4h}{(\alpha^2+4)C_{33}} = \frac{h}{C_{33}}\left(1 - \frac{1}{4}\alpha^2 + O(\alpha^4)\right)\end{aligned}, \tag{18}$$

where $\alpha = k_z h = \frac{2\pi f h}{V}$ and $V = \sqrt{\frac{C_{33}}{\rho}}$ is wave velocity along z direction. From (18), one concludes that the absolute error in the transfer matrix element $\Delta\mathbf{B}[3,7] = \mathbf{B}[3,7] - \mathbf{B}_{\mathrm{II}}[3,7]$ is third order in h: $\frac{1}{12C_{33}} h\alpha^2 = \frac{k_z}{12C_{33}} h^3$. However, because of the absence of a zero order term h^0, the relative error $\Delta\mathbf{B}[3,7]/\mathbf{B}[3,7]$ is $\frac{1}{12}\alpha^2$, i.e., in the second order term h^2. Similarly, one can determine the relative error for other elements of the transfer and stiffness matrices and the average relative error for both matrices is $1/12\alpha^2$.

To estimate the truncation error for wave propagation in an arbitrary direction of a generally anisotropic layer, for $\alpha = k_z h$ we take the upper bound of α by selecting the wave number of the slow quasishear wave with velocity V_{qs} at normal incidence (usually wave propagation in the normal direction has a larger wave number projection k_z than in any other propagation direction), i.e., $\alpha = k_z h \le \frac{2\pi f H}{V_{qs}} 2^{-n}$.

The total relative error is the sum of the truncation and round-off errors. The total relative errors $E(\mathbf{B})$, $E(\mathbf{K})$ for both matrices are written as:

$$E(\mathbf{B}) = \alpha_0 4^{-n} + e_0 2^n,\ E(\mathbf{K}) = \alpha_0 4^{-n} + e_0 4^n, \tag{19}$$

where $\alpha_0 = \frac{1}{3}\left(\frac{\pi f H}{V_{qs}}\right)^2$. The total relative error calculated by (19) is shown by solid lines in Fig. 2; it is in very good agreement with the actual computational error shown by the triangles for the transfer and stiffness matrices of the anisotropic layer. The minimum of the average relative error corresponds to the optimum number n_{opt} of the recursive operations. It is obtained from (19):

$$n_{\text{opt}}(\mathbf{B}) = \frac{1}{3}\left(1 + \log_2 \frac{\alpha_0}{e_0}\right),\ n_{\text{opt}}(\mathbf{K}) = \frac{1}{4}\log_2 \frac{\alpha_0}{e_0}. \tag{20}$$

It provides the optimum number of recursive operations for transfer $n_{\text{opt}}(\mathbf{B})$ and stiffness $n_{\text{opt}}(\mathbf{K})$ matrices at given fH and V_{qs}. At this optimal number, the method error is essentially determined by the round-off error at the optimal number of recursive operations [Figs. 2 and 3(a)].

In the same way as for the second order approximation, one obtains the error estimation for the higher order solutions. The round-off error is independent of the order of approximation [Fig. 3(a)]. The average relative errors $E(\mathbf{B})$, $E(\mathbf{K})$ for the higher order solutions are given as functions of the recursive operation number n:

$$E(\mathbf{B}) = \alpha_p 2^{-pn} + e_0 2^n,\ E(\mathbf{K}) = \alpha_p 2^{-pn} + e_0 4^n, \tag{21}$$

where $p\,(= 4, 6, 8)$ is the approximation order and $\alpha_4 = \frac{1}{6!}(k_z H)^4$, $\alpha_6 = \frac{2}{8!5}(k_z H)^6$ and $\alpha_8 = \frac{1}{10!7}(k_z H)^8$. The minimum of the average relative error on the number of the recursive operations n can be obtained from (21). It provides the optimum number of recursive operations n_{opt} for transfer matrix $n(\mathbf{B})$ and stiffness $n(\mathbf{K})$ calculations at given α_p:

$$\begin{aligned} n_{\text{opt}}(\mathbf{B}) &= \frac{1}{(1+p)}\left(1 + \log_2 \frac{\alpha_p}{e_0}\right), \\ n_{\text{opt}}(\mathbf{K}) &= \frac{1}{(2+p)}\log_2 \frac{\alpha_p}{e_0}. \end{aligned} \tag{22}$$

F. Hybrid Asymptotic Method

As was shown above, the computational error (19), (21) depends on the number of subdivisions of the layer (associated with the layer nondimensional thickness) and the plane wave phase velocity associated with the propagation angle. To take advantage of both methods [the smaller round-off error for the transfer matrix and the stability of the stiffness matrix for larger fH (and/or smaller ω/k_x)], we propose a hybrid ($\mathbf{B}/\mathbf{K}$) method. In this algorithm, we start the recursive procedure using the asymptotic transfer matrix. As a control parameter, at each recursive step we calculate the average of the matrix $\mathbf{B}_a$ diagonal elements:

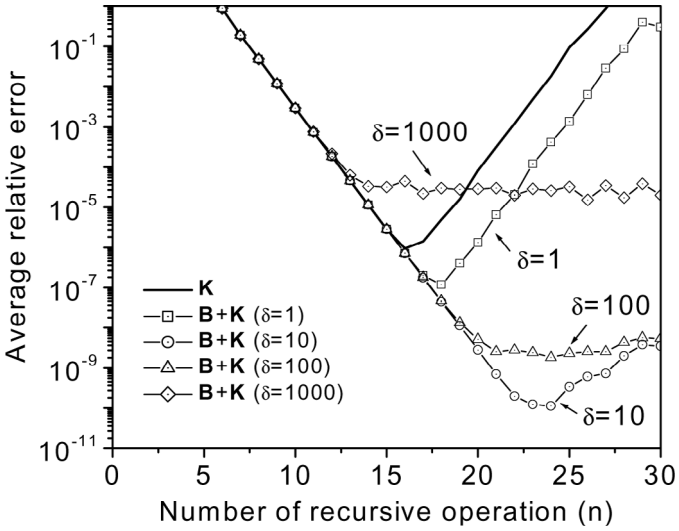

Fig. 4. Average relative error of the hybrid solution for stiffness matrix versus number of recursive operations n for ZnO layer for different values of the control parameter δ (23). fH is 10 GHz*μm. The errors are averaged for phase velocity (ω/k_x) between 0.1 and 20.0 mm/μs.

$$\delta = \frac{1}{8}\sum_{i=1}^{8} |\mathbf{B}_a(i,\, i)|\,. \tag{23}$$

If nonhomogeneous waves exist, the nondimensional parameter δ starts to increase exponentially with the number of recursive operations j (the layer thickness $H_j = 2^j h$). When δ exceeds the selected threshold, we convert the transfer matrix obtained into the stiffness matrix using (12), then continue the recursive operation algorithm using (15); computational instabilities for the $\mathbf{B}_a$ matrix may appear at large δ, thus selecting the proper δ threshold guarantees computational stability.

As an example, we have obtained the total stiffness matrix for a ZnO layer at $fH = 10$ GHz*mm using this hybrid algorithm and recalculated the relative error $E(\mathbf{K})$ shown in Fig. 4 for different δ. $E(\mathbf{K})$ is averaged over the ω/k_x range from 0.1 mm/μs to 40 mm/μs. The relative error for the asymptotic transfer matrix method cannot be obtained for small ω/k_x due to computational instability and is not shown in Fig. 4. The relative error using only the asymptotic stiffness matrix computation ($\delta = 0$) is shown by the solid line. At $\delta = 1$, the round-off error of the hybrid method is smaller than that for the pure stiffness matrix method; it becomes optimal at about $\delta = 10$. With further increase of δ, the minimal error increases.

III. Asymptotic Surface Stiffness Matrix for a Semispace

Above we described the asymptotic solution for computation of a layered structure of finite thickness. For surface acoustic waves (SAW) applications, it is also important to obtain wave propagation solutions for semi-infinite substrates. The exact wave propagation solution for a semi-

space is obtained using the eigenvectors of the acoustic tensor **A** [3], [4]. Thus, if one uses the exact computation for the substrate in the layered system, the simplicity provided by the asymptotic method will be lost. In the framework of our recursive asymptotic method, we may replace the semispace by a thick layer with appropriate wave attenuations. For a sufficiently thick layer, the propagating waves inside the layer attenuate and the layer stiffness matrix converges to the surface stiffness matrix [5], [6]; however, this method could require an excessive number of recursive operations. For this reason, it is advantageous to accelerate the decay of wave amplitudes in the finite-thickness layer. To do so we replace the substrate by a layer with artificial attenuation (PML), which, however, does not change the surface stiffness matrix. The PML concept has been applied in finite element (FEM) computations to replace the absorbing bounding conditions in electromagnetic [14] and elastodynamic [15] problems.

We obtain the governing equation for the PML using the complex stretched coordinates by replacing $\frac{d}{dz}$ by $\frac{d}{\beta dz}$ in (1):

$$\frac{d\xi}{dz} = i\beta \mathbf{A}\xi, \tag{24}$$

where β is a complex variable and **A** is the acoustic tensor for the actual semispace. The transfer matrix solution for such a medium is written in the form of (3) with the replacement of h by $h^* = h\beta$. The introduction of the complex parameter β will not change the eigenvectors and eigenvalues of **A**; for this reason the surface stiffness $\mathbf{K}_S$ of the PML is identical with that for the actual substrate layer with acoustic tensor **A** (the 4×4 surface stiffness matrix $\mathbf{K}_S$ is defined as $\mathbf{T} = \mathbf{K}_S\mathbf{U}$, see Section IV-B and in [6]). Because $\mathbf{K}_S$ is independent of β, the wave behavior at the interfaces between the surface layers and the PML is the same as that for the actual substrate. Because β is complex, all acoustic wave energy transmitted into the PML will be attenuated. The asymptotic transfer and stiffness matrices for the PML layer are obtained by replacing h by h^* in (3), (10) and (13), (14).

In the framework of the PML approach, the procedure to calculate the wave propagation for a semispace is identical to that for the finite thickness layer: we subdivide the layer into thin layers and compute the total transfer or stiffness matrix recursively. The complex parameter β is selected as $(1.0, \beta_i)$ with $0 < \beta_i < 0.5$. As shown in [5], the stiffness submatrices $\mathbf{K}_{12}$ and $\mathbf{K}_{21}$ behave exponentially ($e^{ik_z H}$) for the nonhomogeneous or propagating waves. If one selects the PML thickness H and parameter β from the condition

$$imag\,(k_z H) = \frac{2\pi f H \sin(\theta_x)}{V_{ql}}\beta_i > n_e, \tag{25}$$

where θ_x is the angle between propagation direction and x-axis and V_{ql} is the fastest velocity in this direction, then the wave displacements and stresses at the PML bottom are of order e^{-n_e}. If, for example, one selects n_e as $16 \log_e 10 \approx 37$, then the displacement and stress values on the PML bottom surface will be close to the minimal round-off error e_0 in (17), and the semispace solution satisfies the radiation condition.

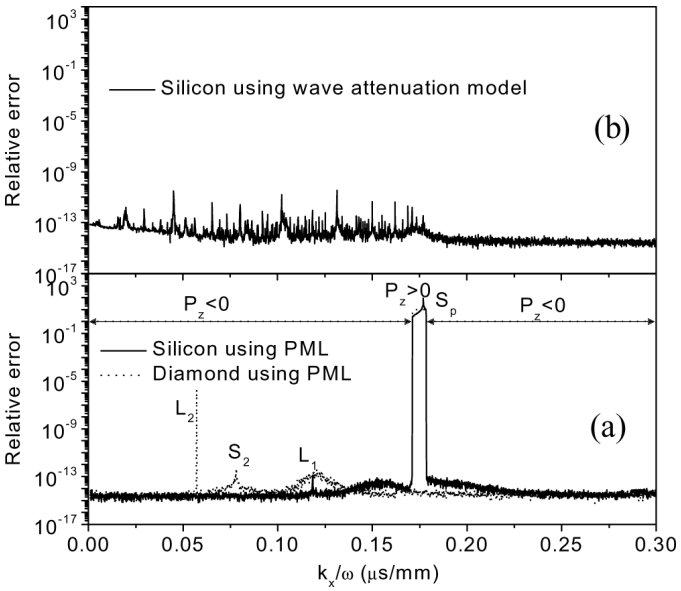

Fig. 5. Relative error $E(\mathbf{K}_S)$ for the asymptotic surface stiffness matrix versus k_x/ω for silicon and diamond substrates. (a) Calculated by the PML method. The PML layer has $fH = 3,000$ GHz$^*\mu$m with $\beta_i = 0.3$. L_1, L_2, S_1, S_2 indicate the critical angles shown in Fig. 6. Sp indicates the anomalous angle sector shown in Fig. 6 for silicon in which phase and group velocities have opposite directions. The solid lines with arrows indicate where the imaginary part of the diagonal terms of the surface stiffness matrix for silicon are all nonpositive $P_z < 0$, anomalous sector marked as positive $P_z > 0$. (b) Relative error calculated when, instead of the PML layer, a finite thickness silicon layer with actual attenuation is used. $fH = 300,000$ GHz$^*\mu$m.

In some methods after replacement of a semispace by absorbing boundary conditions, the solution depends on the wave propagation direction [16]. For example, the paraxial approximation is applicable only for propagation directions close to normal incidence [16]. To investigate the sensitivity of the PML method to wave propagation direction, we have calculated for silicon and diamond substrates the average relative error $E(\mathbf{K}_S)$ between the elements of the exact surface stiffness matrix $\mathbf{K}_S$ for a semispace and elements of the stiffness submatrices $\mathbf{K}_{11}^{\mathrm{PML}}$ for the PML replacement:

$$E(\mathbf{K}_S) = \frac{1}{16}\sum_{i=1}^{4}\sum_{j=1}^{4}\left|\left(\mathbf{K}_{11}^{\mathrm{PML}}[i,\,j] - \mathbf{K}_S[i,\,j]\right)/\mathbf{K}_S[i,\,j]\right|. \tag{26}$$

In both calculations we have used $fH = 3,000$ GHz$^*\mu$m, $\beta_i = 0.3$, and $\delta = 10$ in the hybrid second order method; the number n of recursive operations is 10. As shown in Fig. 5(a), the relative error for the PML solution is very small in all propagation directions except in several isolated regions [peaks in Fig. 5(a)]. To understand these special cases, let us refer to the bulk wave slowness surfaces for silicon and diamond, which are shown in Fig. 6. Comparing Figs. 5(a) and 6, one concludes that the er-

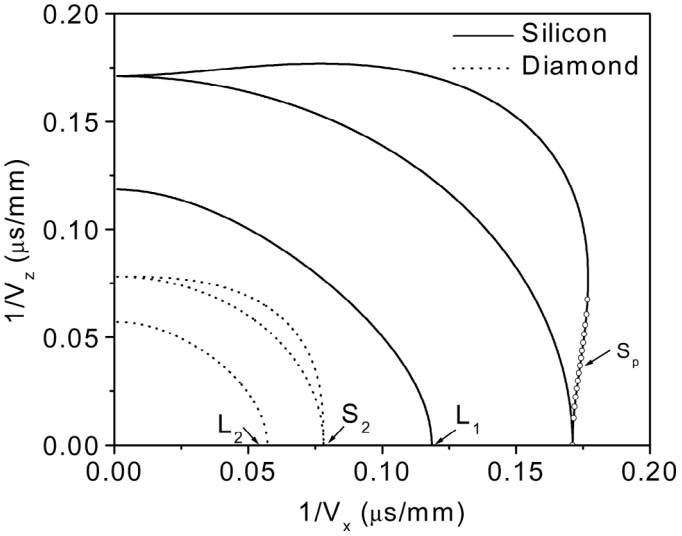

Fig. 6. Slowness surface for silicon (solid lines) and diamond (dotted lines) in one to three plane. L_1, L_2, S_1, S_2 indicate the critical angles. Sp is the anomalous range for the silicon slowness where phase and group velocities have opposite directions.

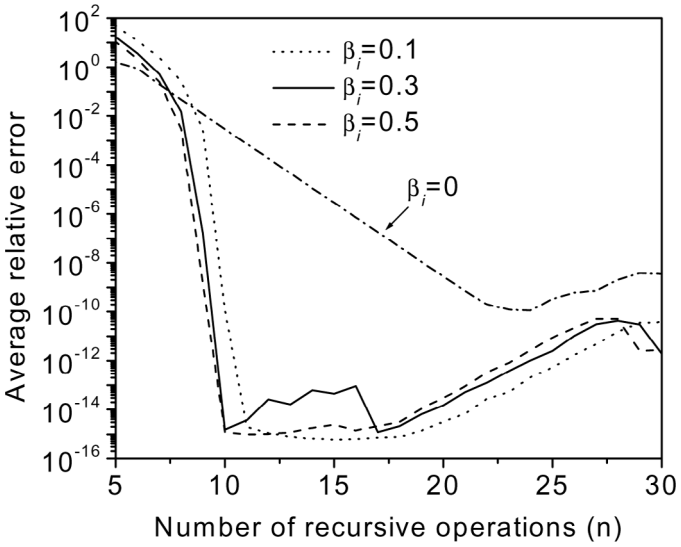

Fig. 7. Average relative error $E(\mathbf{K}_S)$ for the surface stiffness matrix of a diamond semispace using PML model (24) with different complex parameters β. The hybrid method with $\delta = 10$ is used to compute the asymptotic surface stiffness matrix. Frequency is 3,000 GHz. The errors are averaged for phase velocity (ω/k_x) between 1 and 20.0 mm/μs.

ror peaks correspond to the grazing propagation directions when $\theta_x \approx 0$. Adding the actual attenuation in the PML diminishes these peaks. One can see that, for the silicon substrate, there is an additional error peak in the small but finite angle range S_p. This angle range corresponds to the slowness range in which phase and group velocities of the wave carrying energy from the interface have opposite signs (opposite propagation direction along z axis). In this case the complex parameter in (24) (the thickness H^*) taken for the PML results in amplification instead of attenuation of the energy, and the obtained surface stiffness matrix is unphysical. To identify this range, we calculate the energy flow P [17] at the surface:

$$P(z) = \frac{i\omega}{4}\hat{\mathbf{U}}\left(\hat{\mathbf{K}}_S - \mathbf{K}_S\right)\mathbf{U}, \tag{27}$$

where $\hat{}$ means Hermitian conjugate. For a physically acceptable surface stiffness matrix $\mathbf{K}_S$, $P(z)$ must be nonnegative for an upper semispace and nonpositive for a bottom semispace. Therefore, the matrix $\mathbf{K}_S^I = \frac{i\omega}{4}\left(\hat{\mathbf{K}}_S - \mathbf{K}_S\right)$ must be positive semidefinite for an upper semispace and negative semidefinite for a bottom semispace. A rigorous criterion to determine the energy flow direction is the signs of the determinants of the diagonal submatrices of matrix $\mathbf{K}_S^I$. The necessary (but not sufficient) condition for the surface stiffness matrix $\mathbf{K}_S$ to be physically acceptable is that the imaginary part $imag(\mathbf{K}_S(i,i))$ of all the diagonal terms of the surface stiffness matrix $\mathbf{K}_S$ must be nonnegative for an upper semispace and nonpositive for a bottom semispace. Using these criteria, one easily can identify the abnormal part S_p in Fig. 5(a) for silicon. The result is indicated by the solid line with arrows: the $P_z < 0$ part indicates that $imag\left(\mathbf{K}_{11}^{\mathrm{PML}}(i,i)\right)$ for each diagonal term is nonpositive, and the $P_z > 0$ part indicates the angle sector in which one of the $imag\left(\mathbf{K}_{11}^{\mathrm{PML}}(i,i)\right)$ elements is positive. As can be seen, this simple criterion can determine exactly the anomalous angle domain. Within this angle domain, one calculates the surface stiffness matrix using the actual wave attenuation (complex elastic constants) in the substrate layer of finite thickness. The results calculated using the attenuation model are shown in Fig. 5(b). In this calculation the appropriate attenuation [18] in the silicon is introduced, $fH = 300{,}000$ GHz$^*\mu$m is selected and 20 recursive operations are used (the round-off error is higher than that for the PML due to larger layer thickness and correspondingly larger subdivision number n).

As in Fig. 3, we plot in Fig. 7 the relative error $E(\mathbf{K}_S)$ (26) between the exact surface stiffness matrix $\mathbf{K}_S$ for the semispace and the $\mathbf{K}_{11}^{\mathrm{PML}}$ submatrix of the PML layer versus the number of recursive operations n. Calculations are performed for different values of the parameter β_i and $fH = 3{,}000$ GHz$^*\mu$m. The results are obtained using the hybrid method with $\delta = 10$. With increase of n, initially the $\mathbf{K}_{11}^{\mathrm{PML}}$ converges to the exact surface stiffness with the same rate as the stiffness matrix indicated by the dashed lines; however, at n about 8, the convergence rate increases sharply with fast drop of the relative error to e_0. As the number of recursive operations increases further, the round-off error increases with the same rate as for the transfer matrix method shown in Fig. 2.

IV. Applications and Numerical Examples

A. Computational Procedure for a Layered System

For a layered structure, the computational algorithm to obtain the total stiffness matrix recursively is separated into two steps:

- Each homogeneous layer H_m of the layered structure is subdivided into $N = 2^n$ thin layers. Using the asymptotic hybrid recursive algorithm, the layer stiffness $\mathbf{K}_a^m(H_m)$ is obtained.
- Obtain the total stiffness matrix for the layered structure by combining all layer stiffness matrices (including the PML layer) using the stiffness matrix recursive algorithm (see (28), next page) [5], [6], where $\mathbf{K}^M$ are the asymptotic or exact total stiffness matrices for the bottom m layers, $\mathbf{K}_{ij}^{M-1}$ are the submatrices of the total stiffness matrix for the bottom $m-1$ layers, $\mathbf{K}_{ij}^m$ are the submatrices of the mth layer stiffness matrix. Alternatively, the top surface stiffness $\mathbf{K}_S$ [5], [6] for the total system is obtained directly, calculating recursively only the $\mathbf{K}_{11}^M$ $(= \mathbf{K}_S^M)$ submatrix. Because the semi-infinite substrate is replaced by a PML layer, the value of the state vector is negligible at its bottom surface; thus in starting the recursive procedure from the system bottom, the surface stiffness $\mathbf{K}_S^B$ is taken to be zero.

For SAW and sensor applications, one needs to consider the effect of electrodes in the layered piezoelectric system. For a metal layer with high conductivity, the electrical potential ϕ is zero for short-circuit conditions; for this case the stiffness matrix becomes a singular matrix and we use for computation a compliance matrix $\mathbf{S}_t$. For open-circuit conditions for a conductive electrode layer, the electric displacement D_3 is zero and the compliance matrix becomes singular; therefore, in this case we use a stiffness matrix $\mathbf{K}_0$. These matrices are written as:

$$\mathbf{S}_t = \begin{bmatrix} \mathbf{S}_{11}^t & 0 & \mathbf{S}_{12}^t & 0 \\ 0 & 0 & 0 & 0 \\ \mathbf{S}_{21}^t & 0 & \mathbf{S}_{22}^t & 0 \\ 0 & 0 & 0 & 0 \end{bmatrix}, \quad \mathbf{K}_0 = \begin{bmatrix} \mathbf{K}_{11}^0 & 0 & \mathbf{K}_{12}^0 & 0 \\ 0 & 0 & 0 & 0 \\ \mathbf{K}_{21}^0 & 0 & \mathbf{K}_{22}^0 & 0 \\ 0 & 0 & 0 & 0 \end{bmatrix}, \tag{29}$$

where $\mathbf{S}_{ij}^t$ (3×3) and $\mathbf{K}_{ij}^0$ (3×3) are the mechanical compliance and stiffness submatrices respectively [5]. For a thin layer, the elements of the compliance and stiffness matrices are obtained explicitly using the second order asymptotic stiffness matrix (the matrix elements for the compliance matrix are given in Appendix B). For thick isotropic metal layers, we use the analytical stiffness and compliance matrices given in [13].

Using the special compliance/stiffness matrices (29), the electrical short or open (metallized) boundary conditions are naturally included in the recursive stiffness/compliance matrix algorithm. For example, for a layered system with a bottom-free surface and an embedded metal layer with a short-circuit condition on the mth interface, one can start the recursive algorithm from the bottom using the surface stiffness matrix and obtain the total surface stiffness matrix for the structure below the bottom of the metal layer. For this case, one needs to use the compliance matrix $\mathbf{S}_s$ for the layer; therefore, one inverts the total surface stiffness matrix obtained to the compliance matrix at the metal bottom surface. Next one continues the recursive procedure with a recursive compliance (stiffness) matrix algorithm and obtains the total compliance (stiffness) matrix at the top surface of the layered system.

B. Generalized Green's Function and Effective Permittivity of a Layered Substrate

In this section we will discuss results for a layered system on top of a substrate. Let us first define the asymptotic or exact surface stiffness $\mathbf{K}_S$ and compliance $\mathbf{S}_S$ matrices:

$$\begin{bmatrix} \mathbf{u}_n \\ \phi_n \end{bmatrix} = \mathbf{S}_S \begin{bmatrix} \boldsymbol{\sigma}_n \\ D_n \end{bmatrix} = \begin{bmatrix} \mathbf{S}_S^f & \mathbf{S}_S^{fe} \\ \mathbf{S}_S^{ef} & \mathbf{S}_S^e \end{bmatrix} \begin{bmatrix} \boldsymbol{\sigma}_n, \\ D_n \end{bmatrix}, \quad \mathbf{K}_S = \mathbf{S}_S^{-1}. \tag{30}$$

The generalized Green's function $\mathbf{G}_S$ [19], [20] is a 4×4 matrix, which describes the generation of mechanical displacements and electrical potential by mechanical stresses and electrical charge. It is related to the surface compliance matrix $\mathbf{S}_S$ [6]:

$$\begin{bmatrix} \mathbf{u}_n \\ \phi_n \end{bmatrix} = \mathbf{G}_S \begin{bmatrix} \boldsymbol{\sigma}_n \\ \gamma_n \end{bmatrix}; \qquad \mathbf{G}_S = \begin{bmatrix} \mathbf{S}_S^f + \alpha\,|k_x|\,\varepsilon_0 \mathbf{S}_S^{fe}\mathbf{S}_S^{ef} & -\alpha\mathbf{S}_S^{fe} \\ \alpha\mathbf{S}_S^{ef} & -\alpha S_S^e \end{bmatrix}, \tag{31}$$

where $\alpha = 1/\left(1 - |k_x|\,\varepsilon_0 S_S^e\right)$, γ_n is the charge density at the surface and ε_0 is the permittivity of vacuum. The surface effective permittivity is given by:

$$\varepsilon_{eff}\left(k_x, \omega\right) = \frac{\gamma_n}{|k_x|\,\phi_n} = \varepsilon_0 - \frac{1}{|k_x|\,S_S^e}. \tag{32}$$

As an example, we have calculated the effective surface permittivity for a ZnO/diamond/silicon layered semispace using the exact and the second order recursive asymptotic stiffness matrix methods. Fig. 8 shows the real part of the effective surface permittivity versus frequency at the phase velocity 10 mm/μs. The thicknesses of ZnO and diamond layers are 1 μm and 20 μm, respectively. The properties of the materials are listed in Table I and were taken from [20] and the attenuations from [18] and [22]. The imaginary parts of the complex elastic constants c_{ijkl} (Table I) are selected to introduce appropriate longitudinal and shear wave attenuations based on the experimental results [18], [22]. The semispace silicon substrate is represented by the PML layer with $\beta = 1.0 + 0.3i$. The recursive operation number n and the PML layer thickness H are selected based on (20) and (25), respectively. As shown in Fig. 8(b), the relative error of the asymptotic solution is about 10^{-10}. The two peaks marked as R_1 and R_2 represent the SAW modes corresponding to the shorted boundary conditions. At these points the difference between the exact solution and asymptotic solution also becomes larger; however, at these points, both methods have decreased precision due to the presence of poles in the stiffness matrix elements.

C. Velocity of Surface Acoustic Waves

As an additional example, the asymptotic method has been compared to the exact method in the calculation of

$$\mathbf{K}^M = \begin{bmatrix} \mathbf{K}_{11}^m + \mathbf{K}_{12}^m \left(\mathbf{K}_{11}^{M-1} - \mathbf{K}_{22}^m\right)^{-1} \mathbf{K}_{21}^m & -\mathbf{K}_{12}^m \left(\mathbf{K}_{11}^{M-1} - \mathbf{K}_{22}^m\right)^{-1} \mathbf{K}_{12}^{M-1} \\ \mathbf{K}_{21}^{M-1} \left(\mathbf{K}_{11}^{M-1} - \mathbf{K}_{22}^m\right)^{-1} \mathbf{K}_{21}^m & \mathbf{K}_{22}^{M-1} - \mathbf{K}_{21}^{M-1} \left(\mathbf{K}_{11}^{M-1} - \mathbf{K}_{22}^m\right)^{-1} \mathbf{K}_{12}^{M-1} \end{bmatrix}, \tag{28}$$

TABLE I
MATERIAL LAYER PROPERTIES [21].[1]

	ZnO	Diamond	Silicon
C_{11} (GPa)	209.6−0.198i	1076−0.0187i	166−0.0417i
C_{33}	210.6−0.199i	1076−0.0187i	166−0.0417i
C_{44}	42.3−0.008i	575.8−0.002i	79.6−0.004i
C_{12}	120.5−0.114i	125−0.0022i	63.9−0.016i
C_{23}	104.6−0.099i	125−0.0022i	63.9−0.016i
e_{14} (C/m^2)	0	0	0
e_{15}	−0.59	0	0
e_{31}	−0.48	0	0
e_{33}	1.32	0	0
$\varepsilon_{11}/\varepsilon_0$	8.55	5.67	11.7
$\varepsilon_{22}/\varepsilon_0$	8.55	5.67	11.7
$\varepsilon_{33}/\varepsilon_0$	10.2	5.67	11.7
Density (10^3 kg/m^3)	5.68	3.512	2.33

[1]The imaginary parts of the complex elastic constants are selected based on the measured attenuations given in [18] and [22].

the surface wave velocity. The free SAW velocity for a ZnO/diamond/silicon layered semispace has been calculated as poles of the exact and asymptotic surface Green's function (31). All material parameters (Table I) are as those used in Fig. 8. The free-surface wave dispersion curves are shown in Fig. 9. The results obtained by the exact method are shown by solid lines and asymptotic results by open circles. The difference in the velocities calculated by the two methods is about the average error for the Green's function shown in Fig. 8(b) when the absolute error of the stopping criterion in the root search algorithm is smaller than this value. The surface wave velocity also may be computed from the poles and zeros of the effective permittivity. The poles of $\varepsilon_{eff}(k_x, \omega)$ are associated with modes for shorted boundary conditions and the zeros with modes for free-circuit boundary conditions on the surface.

V. Conclusions

We have presented a simple computational method for wave propagation in layered piezoelectric media. In this method, the total transfer and stiffness matrices for a thick layer or multilayers are calculated by subdividing the layers into $N = 2^n$ thin sublayers and combining the thin layer transfer and stiffness matrices by n recursive operations. For thin layers, explicit asymptotic transfer and stiffness matrices are formulated for the case of general anisotropy and piezoelectricity. This asymptotic representation of the sublayers maintains the energy balance of the propagating wave and system homogeneity, i.e., assures absence of scattering on the subdivided layer interfaces. It is shown that the method converges both analytically and computationally to the exact transfer and stiffness matrices of the layered structure. Analysis of computational error introduced by truncation and rounding off has been given. To estimate a priori the optimal number N_{opt} of layer subdivisions, we obtained simple equations that depend only on layer thickness, frequency, and shear wave velocity. At N_{opt} the error of the method is the computational round-off error determined by the computer precision. The truncation error is the same for both methods. But the round-off error of the stiffness recursive algorithm is twice that of the transfer matrix, and the precision of the stiffness matrix method is higher for thicker layers. For this reason, a hybrid method that uses the transfer matrix in the beginning of the recursive operation for thin layers and the stiffness matrix for thick layers has been proposed. The control parameter for this transition has been suggested.

For a semispace substrate, a PML method has been introduced and implemented. It was found that the PML method is inapplicable in the small angle domain in which the phase and group velocities of the quasitransverse partial wave in the semispace are in opposite directions. A simple criterion based on the positive semidefinite property of the surface stiffness matrix has been given to identify those domains. For computations in this abnormal angle domain, we have used a thick substrate with an actual attenuation to replace the semispace. Examples for computation of the surface Green's function and the effective surface permittivity for a layered substrate and the SAW velocity for a layered semispace are given to demonstrate the method's applicability. We find that the advantage of the asymptotic method is its simplicity and efficiency.

Appendix A
Fundamental Acoustic Tensor A

The fundamental acoustic tensor $\mathbf{A}$ for a piezoelectric medium is represented as [3], [4]:

$$\mathbf{A} = \begin{bmatrix} k_x \mathbf{X} \boldsymbol{\Gamma}_{31} & -i\mathbf{X} \\ -i\left(\boldsymbol{\Gamma}_{11} - \boldsymbol{\Gamma}_{13}\mathbf{X}\boldsymbol{\Gamma}_{31}\right) k_x^2 + i\rho\omega^2 \mathbf{I}' & k_x \boldsymbol{\Gamma}_{13}\mathbf{X} \end{bmatrix}, \tag{A1}$$

where ρ is the density of the solid and $\boldsymbol{\Gamma}_{ik}$ are the 4×4 matrices formed from the elastic constants c_{ijkl}, piezoelectric stress constants e_{ijk}, and dielectric permittivity constants ε_{ik}:

$$\boldsymbol{\Gamma}_{ik} = \begin{bmatrix} c_{1i1k} & c_{1i2k} & c_{1i3k} & e_{k1i} \\ c_{2i1k} & c_{2i2k} & c_{2i3k} & e_{k2i} \\ c_{3i1k} & c_{3i2k} & c_{3i3k} & e_{k3i} \\ e_{i1k} & e_{i2k} & e_{i3k} & -\varepsilon_{ik} \end{bmatrix}. \tag{A2}$$

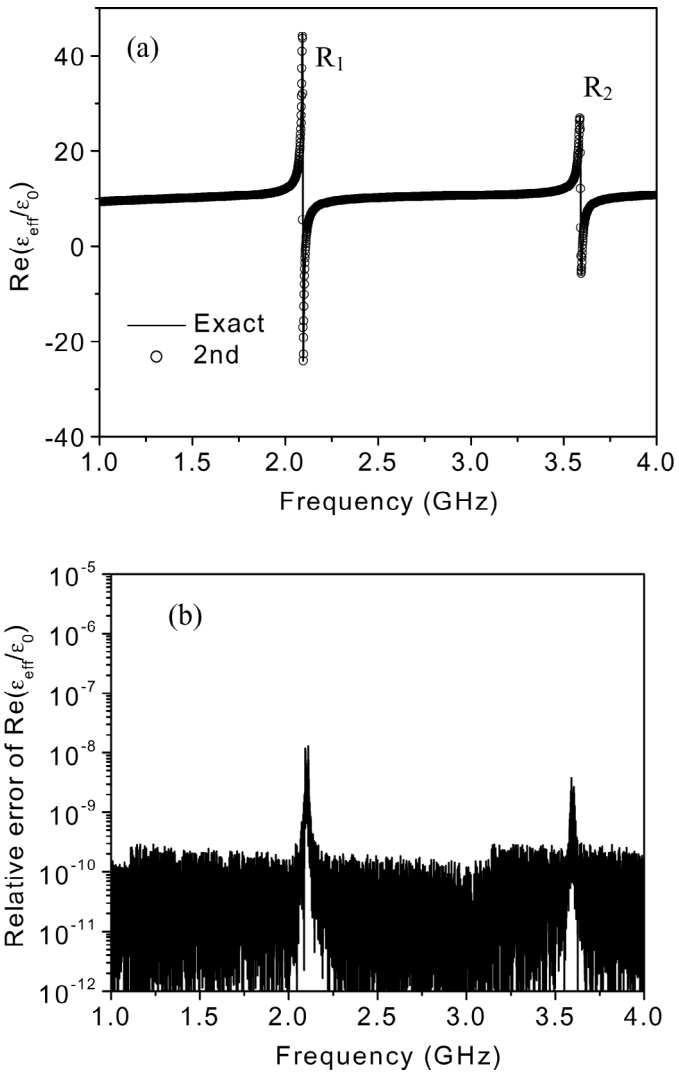

Fig. 8. (a) Effective surface permittivity for a ZnO/diamond/silicon layered semispace versus frequency calculated by the asymptotic (open circles) and exact (solid line) methods at phase velocity 10 mm/μs. Thickness of ZnO and diamond layers is 1 μm and 20 μm, respectively. In exact computation, silicon is a semispace. In the asymptotic calculation, the semispace silicon substrate is represented by the PML layer. (b) Relative error in the surface permittivity computation.

$\mathbf{X}$ is the inverse matrix of $\mathbf{\Gamma}_{33}$: $\mathbf{X} = \mathbf{\Gamma}_{33}^{-1}$, $\mathbf{I}'$ is the 4×4 identity matrix but with zero $(4,4)$ element.

Appendix B
Second Order Compliance Matrix for an Isotropic Thin Conductive Layer

The acoustic tensor for an isotropic conducting layer can be written as (B1) (see next page). Using the second order asymptotic stiffness or transfer matrix for an isotropic material, the second order compliance matrix for an isotropic conductive layer is obtained as (B2) and (B3) (see next page), where $C = \rho\omega^2 C_{11} - 4k_x^2 C_{44}\,(C_{11} - C_{44})$, $C_{11} = \rho V_l^2$ and $C_{44} = \rho V_t^2$, and V_l, V_t are longitudinal and shear velocities. Following from the symmetry properties in this appendix, the submatrices $\mathbf{S}_{22}^t = -\left(\mathbf{S}_{11}^t\right)^T$ and $\mathbf{S}_{21}^t = -(\mathbf{S}_{21}^t\hat{)}$.

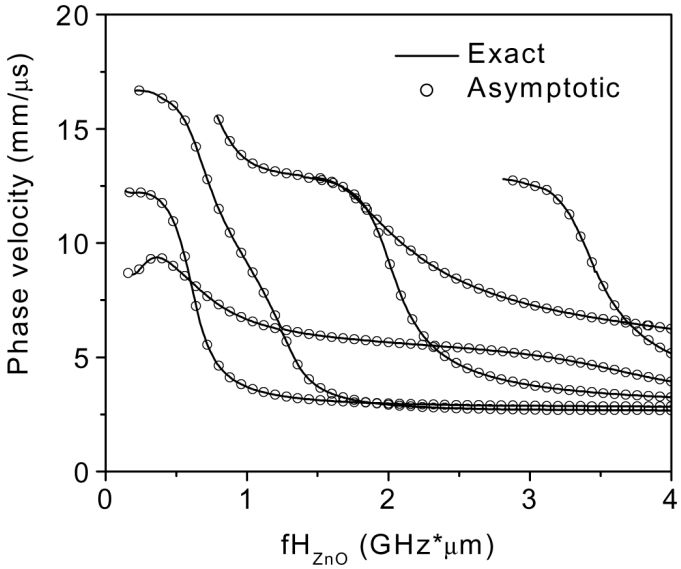

Fig. 9. Surface wave velocity calculation for the ZnO/diamond/silicon layered semispace using exact (solid lines) and asymptotic (open circles) surface stiffness matrix. Material parameters are the same as those used in Fig. 8. In the asymptotic computation, the silicon semispace is replaced by the PML.

References

[1] L. Wang and S. I. Rokhlin, "Recursive asymptotic stiffness matrix method for analysis of surface acoustic wave devices on layered piezoelectric media," *Appl. Phys. Lett.*, vol. 81, pp. 4049–4052, 2002.

[2] S. I. Rokhlin and W. Huang, "Ultrasonic wave interaction with a thin anisotropic layer between two anisotropic solids: II. Second-order asymptotic boundary condition," *J. Acoust. Soc. Amer.*, vol. 94, pp. 3405–3420, 1993.

[3] A. H. Fahmy and E. L. Adler, "Propagation of acoustic waves in multilayers: A matrix description," *Appl. Phys. Lett.*, vol. 20, pp. 495–497, 1973.

[4] E. L. Adler, "SAW and pseudo-SAW properties using matrix methods," *IEEE Trans. Ultrason., Ferroelect., Freq. Contr.*, vol. 41, pp. 876–882, 1994.

[5] S. I. Rokhlin and L. Wang, "Stable recursive algorithm for elastic wave propagation in layered anisotropic media: Stiffness matrix method," *J. Acoust. Soc. Amer.*, vol. 112, pp. 822–834, 2002.

[6] L. Wang and S. I. Rokhlin, "A compliance/stiffness matrix formulation of general Green's function and effective permittivity for piezoelectric multilayers," *IEEE Trans. Ultrason., Ferroelect., Freq. Contr.*, vol. 51, pp. 453–463, 2004.

[7] K. E. Pauley and S. B. Dong, "Surface acoustic wave properties in ZnO-SiO_2-Si layered structure," *Wave Electron.*, vol. 1, pp. 265–285, 1976.

[8] E. Kausel, "Wave propagation in anisotropic layered media," *Int. J. Numer. Methods Eng.*, vol. 23, pp. 1567–1578, 1986.

[9] S. K. Datta, *Comprehensive Composite Materials*. vol. 1, T. W. Chou, Ed. Amsterdam, The Netherlands: Elsevier, 2000, pp. 511–558.

[10] J. H. Wilkinson, *Round off Errors in Algebraic Processes*. Englewood Cliffs, NJ: Prentice-Hall, 1963.

[11] L. Wang and S. I. Rokhlin, "Recursive geometric integrators for wave propagation in a functionally-graded multilayered elastic medium," *J. Mech. Phys. Solids*, 2004, to be published.

[12] P. Wynn, "On the convergence and stability of the Epsilon algorithm," *J. SIAM Numer. Anal.*, vol. 3, pp. 91–122, 1966.

$$\mathbf{A} = \begin{bmatrix} 0 & 0 & 1 & \frac{1}{iC_{44}} & 0 & 0 \\ 0 & 0 & 0 & 0 & \frac{1}{iC_{44}} & 0 \\ -\frac{k_x C_{13}}{C_{11}} & 0 & 0 & 0 & 0 & \frac{1}{iC_{11}} \\ i\left(\rho\omega^2 - Q_{11}k_x^2\right) & 0 & 0 & 0 & 0 & -\frac{k_x C_{13}}{C_{11}} \\ 0 & i\left(\rho\omega^2 - Q_{66}k_x^2\right) & 0 & 0 & 0 & 0 \\ 0 & 0 & i\rho\omega^2 & 1 & 0 & 0 \end{bmatrix}. \tag{B1}$$

$$\mathbf{S}_{11}^t = \begin{bmatrix} \frac{C_{11}}{hC} - \frac{h}{4}\left(\frac{1}{C_{44}} - \frac{k_x^2}{\rho\omega^2}\right) & 0 & \frac{ik_x C_{44}\left(\rho\omega^2 - 2k_x^2(C_{11}-C_{44})\right)}{\rho\omega^2 C} \\ 0 & \frac{1}{h(\rho\omega^2 - k_x^2 C_{44})} - \frac{h}{4C_{44}} & 0 \\ -\frac{ik_x C_{44}\left(\rho\omega^2 - 2k_x^2(C_{11}-C_{44})\right)}{\rho\omega^2 C} & 0 & \frac{1}{h\rho\omega^2} - \frac{h\left(\rho\omega^2 - k_x^2 C_{11}\right)}{4C} \end{bmatrix}, \tag{B2}$$

$$\mathbf{S}_{12}^t = \begin{bmatrix} -\frac{C_{11}}{hc} - \frac{h}{4}\left(\frac{1}{C_{44}} - \frac{k_x^2}{\rho\omega^2}\right) & 0 & -\frac{ik_x\left(\rho\omega^2 - 2k_x^2 C_{44}\right)(C_{11}-C_{44})}{\rho\omega^2 C} \\ 0 & -\frac{1}{h(\rho\omega^2 - k_x^2 C_{44})} - \frac{h}{4C_{44}} & 0 \\ -\frac{ik_x\left(\rho\omega^2 - 2k_x^2 C_{44}\right)(C_{11}-C_{44})}{\rho\omega^2 C} & 0 & -\frac{h}{\rho\omega^2} - \frac{h\left(\rho\omega^2 - k_x^2 C_{11}\right)}{4C} \end{bmatrix}, \tag{B3}$$

[13] L. Wang and S. I. Rokhlin, "Stable reformulation of transfer matrix method for wave propagation in layered anisotropic media," *Ultrasonics*, vol. 39, pp. 407–418, 2001.

[14] J. P. Berenger, "A perfectly matched layer for the absorption of electromagnetic waves," *J. Comput. Phys.*, vol. 114, pp. 185–200, 1994.

[15] W. C. Chew and Q. H. Liu, "Perfectly matched layers for elastodynamics: A new absorbing boundary condition," *J. Comput. Acoust.*, vol. 4, pp. 72–79, 1996.

[16] E. Kausel and G. Manolis, *Wave Motion in Earthquake Engineering*. Boston: WIT Press, 2000.

[17] B. A. Auld, *Acoustic Fields and Waves in Solids*. New York: Wiley, 1973.

[18] B. G. Helme and P. S. King, "The phonon viscosity tensor of Si, Ge, GaAs and InSb," *Phys. Status Solidi A*, vol. 45, pp. 33–39, 1978.

[19] R. C. Peach, "A general Green function analysis for SAW devices," in *Proc. IEEE Ultrason. Symp.*, 1995, pp. 221–225.

[20] R. C. Peach, "On the existence of surface acoustic waves on piezoelectric substrates," *IEEE Trans. Ultrason., Ferroelect., Freq. Contr.*, vol. 48, pp. 1308–1320, 2001.

[21] A. J. Slobodnik, E. D. Conway, and R. T. Delmonico, *Microwave Acoustics Handbook*. vol. 1A, Springfield: Surface Wave Velocities, TR-73-0597, AD780172, NTIS, 1973.

[22] D. H. R. Price and C. D. W. Wilkinson, "Frequency dependence of ultrasonic attenuation in zinc oxide at room temperature," *Appl. Phys. Lett.*, vol. 16, pp. 504–507, 1970.

Lugen Wang received his B.S. degree from the University of Science and Technology of China, Hefei, China, in electrical engineering in 1992 and Ph.D. degree from The Ohio State University, Columbus, in industrial, welding and systems engineering in 2001. He began his research career in the Institute of Acoustics, Chinese Academy of Science, Beijing, China, where he performed research in acoustic imaging.

Since 2001, he has been with the Nondestructive Evaluation (NDE) Lab in The Ohio State University as a research scientist. His primary research interests are wave propagation, NDE, acoustic imaging, atomic and acoustic microscopes.

Dr. Wang is a member of the IEEE, American Society for Nondestructive Testing, and Acoustic Society of America.

Stanislav I. Rokhlin is a professor in the Department of Industrial, Welding and Systems Engineering at The Ohio State University (OSU), Columbus. He joined the faculty at OSU in 1985.

His research interests are in the areas of ultrasonic wave propagation and characterization of inhomogeneous and anisotropic materials, including composites and adhesive bonds, and interphase mechanics and environmental degradation and failure. He also is active in the fields of sensors for material process control, acoustic emission and microfocal x-ray radiography, and tomography. He has several patents, has authored over 250 publications, and has given numerous presentations.

Dr. Rokhlin received the Charles H. Jennings Memorial Medal Award from the American Welding Society (AWS) in 1986; the Alcoa Foundation Award in 1988 and 1989; the A. F. Davis Silver Medal Award from AWS in 1991; the Faculty Research Award in 1990, 1994, and 1998 from OSU; in 1996 the National Aeronautics and Space Administration (NASA) Technical Recognition Award; and in 1988 the American Society of Nondestructive Testing (ASNT) Outstanding Paper Award. Dr. Rokhlin is a member of ASNT, AWS, and the American Society of Mechanical Engineers (ASME) and served on several committees for these societies. He is a Fellow of the Acoustical Society of America (ASA). He is an associate editor of *Materials Evaluation* and on the Editorial Boards of *Research in NDE* and *Journal of NDE*. He has served as Guest Editor for several special issues on nondestructive evaluation topics for different journals and has been the organizer of several professional meetings. He also has served on the ASNT Board of Directors and has been on the Editorial Board of the *Journal of Adhesion Science and Technology*.